



Published in final edited form as:

Biochemistry. 2011 March 1; 50(8): 1412–1420. doi:10.1021/bi101900b.

Transition State Analysis of the Arsenolytic Depyrimidination of Thymidine by Human Thymidine Phosphorylase†

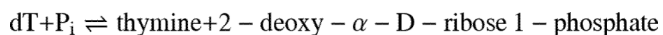
Phillip A. Schwartz, Mathew J. Vetticatt, and Vern L. Schramm*

* Department of Biochemistry, Albert Einstein College of Medicine, 1300 Morris Park Avenue, Bronx, NY 10461, Phone 718-430-2813, Fax 718-430-8565

Abstract

Human thymidine phosphorylase (hTP) is responsible for thymidine (dT) homeostasis, promotes angiogenesis, and is involved in metabolic inactivation of antiproliferative agents that inhibit thymidylate synthase. Understanding its transition state structure is on the path to design transition state analogues. Arsenolysis of dT by hTP permits kinetic isotope effect (KIE) analysis of the reaction by forming thymine and the chemically unstable 2-deoxyribose 1-arsenate. The transition state for the arsenolytic reaction was characterized using multiple KIEs and computational analysis. Transition state analysis revealed a concerted bimolecular (A_ND_N) mechanism. A transition state constrained to match the intrinsic KIE values was found using density functional theory [B3LYP/6-31+G*]. An active site histidine is implicated as the catalytic base responsible for activation of the arsenate nucleophile and stabilization of the thymine leaving group during the isotopically sensitive step. At the transition state, the deoxyribose ring exhibits significant oxocarbenium ion character with bond-breaking ($r_{C-N} = 2.45 \text{ \AA}$) nearly complete but no significant bond-making to the attacking nucleophile ($r_{C-O} = 2.95 \text{ \AA}$). The transition state model predicts a deoxyribose conformation with a 2'-endo ring geometry. Transition state structure for the slow hydrolytic reaction of hTP involves a stepwise mechanism (Schwartz, P.A., Vetticatt, M.J., Schramm, V.L. (2010) *J. Am. Chem. Soc.* 132, 13425–13433), in contrast to the concerted mechanism described here for arsenolysis.

Human thymidine phosphorylase (hTP)¹ catalyzes the reversible phosphorolytic depyrimidination of thymidine (dT) (1,2):



Arsenate is a substrate analogue of phosphate and reduces the reverse reaction to permit transition state analysis by kinetic isotope effects (KIEs) (see *commitments to catalysis*). The hTP-catalyzed arsenolytic depyrimidination of dT forms an unstable 2-deoxy- α -D-ribose 1-arsenate which undergoes spontaneous hydrolysis (Fig. 1).

hTP is involved in dT homeostasis by participating in pyrimidine salvage (3,4). The enzyme is also involved in promoting angiogenesis (5–7). hTP is linked to angiogenesis by the production of 2-deoxyribose (dRib) from dT, a chemoattractant that stimulates the

†Supported by NIH Research Grant GM41916

*Address correspondence to vern.schramm@einstein.yu.edu.

Supporting Information Available: Arsenolytic kinetic data and the complete calculation results are available in the supporting information available free of charge via the Internet at <http://pubs.acs.org>.

¹Abbreviations: dRib, 2-deoxyribose; dT, thymidine; EIE, equilibrium isotope effect; hTP, human thymidine phosphorylase; KIEs, kinetic isotope effects.

endothelial cell migration for new capillary formation (8,9). Angiogenesis is essential in the progression of solid tumors, as they fail to grow beyond a few mm³ without a capillary bed to meet demands for nutrients and oxygen (10). hTP inhibition is proposed to halt the angiogenesis required for tumor hyperproliferation (11). hTP also degrades antiproliferative agents including 5-trifluorothymidine (TFT) and 2'-deoxy-5-fluorouridine (5FdU), compounds designed to inhibit thymidylate synthase, an enzyme crucial in *de novo* DNA synthesis (12–14). Administration of an hTP inhibitor in combination with these drugs increases their efficacy, permitting reduced dose and decreased off-target toxicity (15).

Transition state analysis has been used to design transition state analogues in other N-ribosyltransferases (16). A common feature for N-ribosidic bond cleavage reactions of nucleosides and nucleotides is the appearance of an oxocarbenium ion intermediate (stepwise process) or a transition state exhibiting oxocarbenium ion character (concerted bimolecular process) (Fig. 2) (17). The majority of these reactions proceed through highly dissociative concerted A_ND_N mechanisms² where leaving group departure is advanced before nucleophile approach (18–22). Stepwise mechanisms predominantly involve 2-deoxyribose where all 2-deoxyribose hydrolysis reactions are stepwise. Base excision repair enzymes uracil DNA glycosylase (23,24) and MutY (25) proceed through stepwise D_N[‡]*A_N and D_N*A_N[‡] mechanisms, respectively. Ricin A-chain catalyzes the depurination of small stem-loop DNA in a D_N[‡]*A_N reaction (26). Recent studies reveal that the hTP-catalyzed hydrolysis of dT involves a stepwise D_N*A_N[‡] process (27).

Here, the arsenolytic depyrimidination of dT by hTP is documented kinetically and by multiple KIEs. hTP catalyzes a concerted, dissociative A_ND_N mechanism reaction with ribooxocarbenium ion character at the transition state. Important hydrogen bond interactions between the nucleophile and the leaving group to active site His 116 facilitates catalysis.

EXPERIMENTAL PROCEDURES

Materials

³H- and ¹⁴C- labeled riboses and glucoses and [5'-³H]dT were purchased from American Radiolabeled chemicals. ¹⁵N-labeled thymine was a generous gift from Industrial Research Limited (Lower Hutt, New Zealand). Tetrabutylammonium bisulfate (Fluka), and 2-deoxyribose (dRib, Acros) were purchased commercially. Ultima Gold scintillation fluid (Perkin-Elmer) was used for all scintillation counting. Acetonitrile, methanol, trifluoroacetic acid, and 14.6 cm glass Pasteur pipettes for charcoal columns were purchased from Fisher. Ribonucleotide-triphosphate reductase was a generous gift from Dr. Gary Gerfen (Albert Einstein College of Medicine) (28). Ribokinase (29), phospho-D-ribose-1-pyrophosphate synthase (29), and adenine phosphoribosyltransferase (30) were prepared as described previously. All other reagents and synthetic enzymes were from Sigma-Aldrich.

The gene encoding hTP was subcloned into a pTWIN1 expression vector (New England Biolabs) and overexpressed in the K BR2566 (T7 express) cell strain of *Escherichia coli* (New England Biolabs). hTP was purified as described elsewhere (27) and concentrated by ultrafiltration to ~ 20 mg/mL as determined by the calculated molar extinction coefficient of 23,490 M⁻¹ cm⁻¹ at 280 nm with a specific activity of 10 U/mg at 22 °C for the phosphorolysis of dT. This construct and associated after-expression processing generates

²In IUPAC nomenclature, a reaction mechanism is symbolized by dividing the reaction into elementary steps. D_N represents nucleofuge dissociation and A_N represents nucleophile addition. When D_N and A_N occur in separate steps, and a discrete intermediate is formed (stepwise mechanism), the terms are separated by an asterisk (*) if the intermediate is too short-lived to diffusionally separate from the leaving group. Furthermore, the superscript “‡” denotes which step is the rate limiting chemical step. In a bimolecular reaction, when A_N and D_N occur in the same step (concerted mechanism), the terms are not separated (A_ND_N).

the native amino acid sequence encoded by human mRNA for hTP. Stock enzyme was stored in 20 mM phosphate pH 7.4. Before use, stock enzyme was thawed on ice, inserted into a 0.5 mL slide-a-lyzer dialysis cassette, and dialyzed against argon-saturated 20 mM HEPES pH 7.4 buffer at 4 °C with 7 × 300 mL exchanges over 20 hours. A constant stream of argon was bubbled through the buffer during dialysis.

Analytical Methods

hTP activity was monitored by spectrophotometer (Cary 300) in a 1 cm⁻¹ path length quartz cuvette containing 1 mL of 20 mM HEPES pH 7.4, 50 mM potassium phosphate (or 10 mM sodium arsenate), 1 mM dT, and ~ 50 nM hTP. The reaction progress was monitored by the decrease in absorbance of dT upon depyrimidination at 290 nm using an extinction coefficient of $\Delta\epsilon_{290} = 1000 \text{ M}^{-1} \text{ cm}^{-1}$.

Steady-State Parameters for hTP Arsenolysis

A model SX-20 stopped-flow spectrometer (Applied Photophysics) outfitted with a mercury-xenon lamp was used to follow the arsenolytic depyrimidination of dT by hTP in order to capture the initial velocity period of the steady state at low substrate concentrations, while still maintaining enough hTP to accurately measure a rate. In the reaction chamber, 20 mM HEPES pH 7.4, 1 mM DTT, and varying concentrations of dT or sodium arsenate under saturating concentrations of the second substrate (2.5 mM sodium arsenate or 0.5 mM dT, respectively) were monitored for hTP-catalyzed arsenolysis using the parameters described above (see *analytical methods*). hTP concentration was maintained at 175 nM (22 °C) or 90 nM (37 °C) in the assay. Apparent K_m 's and k_{cat} were determined using the Michaelis-Menten equation.

Synthesis of radiolabeled dT

Except for the 5'-³H and 2'-³H labels, dTs were synthesized enzymatically in three steps via ATP and dATP based on an enzymatic synthesis described previously (31). The exact experimental procedure used for this enzymatic synthesis has been reported (27).

Glucose or ribose was converted into ATP through the action of adenine phosphoribosyltransferase, phospho-D-ribosyl-1-pyrophosphate synthase, pyruvate kinase, and myokinase. In reactions starting from glucose additional enzymes were added: hexokinase, glucose-6-phosphate dehydrogenase, phosphogluconic acid dehydrogenase, phosphoriboisomerase, and glutamate dehydrogenase. In reactions starting from ribose, ribokinase was present. Radiolabeled ATP was converted into dATP using class II ribonucleotide-triphosphate reductase. dATP was converted to dT in a two part procedure previously described using hexokinase, myokinase, adenosine deaminase, alkaline phosphatase, hTP, purine nucleoside phosphorylase, and xanthine oxidase (32).

2'-³H labels were synthesized enzymatically from specifically radiolabeled dRib with ribokinase, phosphoglucomutase, and hTP. 5'-³H labeled dT was commercially available. Labels and their starting material can be found in Table 1 and the original synthetic procedure is documented elsewhere (27).

Determination of KIEs by Scintillation Counting

Competitive KIEs for substrate isotopically enriched with either ³H or ¹⁴C at various positions were measured for the arsenolytic reaction catalyzed by hTP. The isotopic label of interest was mixed with the remote label listed in Table 1 at a CPM ratio of 2:1 ³H:¹⁴C. KIEs were determined by measuring the difference in the ³H/¹⁴C ratio of products from a partially reacted sample and a reaction taken to completion (33). Two 200 μL reactions in 20 mM HEPES pH 7.4 were run in parallel, the partially reacted and the completely reacted

samples, and augmented with 100 μM or 10 mM sodium arsenate, respectively. A master mix containing the appropriate pair of radiolabels (5×10^5 cpm of ^{14}C) and cold carrier was used to make each sample 100 μM dT. The reactions were initiated with the addition of either 5 nM hTP to the partially reacted sample or 300 nM hTP to the completely reacted sample. After incubation for 1 h at 37 $^\circ\text{C}$, 40 μL aliquots (6 from each reaction mixture) were loaded onto activated charcoal columns poured in 14.6 cm glass Pasteur pipettes plugged with glass wool. Charcoal columns contained ~ 1.3 mL of a 4:1 cellulose/charcoal resin poured from a slurry in 10 mM dRib wash buffer. After the sample entered the charcoal bed, the wall of the pipette was rinsed with 3×40 μL of wash buffer. One mL of wash buffer was added to the column and eluted. The wash step was followed by 3×1 mL elution steps using wash buffer augmented with 10% ethanol. All elution steps from one column were collected directly into one scintillation vial. Samples were dried on a speed-vac, resuspended in 200 μL of H_2O , mixed with 10 mL of scintillation fluid, and measured by scintillation counting.

$^3\text{H}/^{14}\text{C}$ ratios were determined by counting samples for 10×5 min in a dual channel scintillation detector (Wallac Winspectral model 1414) and using an appropriate ^{14}C standard to relate channel cpm to total cpm from either radiolabel. Complete reaction in the appropriate sample was verified by the reversed-phase HPLC on a small aliquot quenched in 2 μL of TFA (27). The fractional extent of the reaction was determined both chromatographically, in a similar fashion to the completely reacted sample and radiometrically, by comparing the remote label in the partially and completely reacted samples. Observed KIEs were calculated according to eq 1.

$$\text{KIE} = \frac{\log(1 - f)}{\log(1 - f)(R_p/R_0)} \quad (1)$$

Where f is the fractional extent of the reaction and R_p and R_0 are the isotope ratios in the product at fractional and total reaction, respectively.

Competitive KIEs using a remote label are a function of the apparent KIEs for both labeled and remote labeled substrate. The measured KIE for $5'\text{-}^{14}\text{C}$ was assumed to be unity as it is three bonds removed from the reaction center and ^{14}C does not manifest significant isotope effects for geometric changes or binding (in contrast to remote ^3H labels) (34,35). The KIE for the position of interest was calculated by first determining the KIE for the remote ^3H label and using that value to correct the observed KIE. Radiolabeled substrates and the remote labels used are listed in Table 1. The apparent KIE for the ^3H label used a separate experiment with $[5'\text{-}^{14}\text{C}]\text{dT}$ as the remote label. Apparent KIEs for the positions at or near the reaction coordinate were calculated according to eq 2.

$$\text{KIE}_{\text{app}} = \text{KIE}_{\text{obs}} \times \text{KIE}_{\text{remote}} \quad (2)$$

KIE_{app} is the apparent KIE for the position of interest, KIE_{obs} is the experimentally measured KIE, and $\text{KIE}_{\text{remote}}$ is the observed KIE for the remote label.

Computational analysis

The arsenolytic reaction of thymidine catalyzed by hTP was studied using B3LYP method with a 6-31G* basis set as implemented in Gaussian 09. Reactant, intermediate, and product geometries were located as global minima and frequency calculations performed on these

optimized geometries had no imaginary frequencies. Most transition state structures, located with and without geometric constraints, were found to have only one imaginary frequency, characteristic of true potential energy saddle points. The errors associated with isotope effect predictions for geometries with more than one imaginary frequency are discussed elsewhere (37). Isotope effects were calculated for each of these transition structures using ISOEFF 98 (38). For the final model, a one-dimensional infinite parabola correction was applied to account for tunneling contributions (39).

RESULTS

Steady-state Kinetic Parameters for hTP-Catalyzed Arsenolysis

Kinetic parameters for the arsenolytic depyrimidination of dT by hTP were measured using a stopped-flow spectrophotometer. Data followed Michaelis-Menten type kinetics and values for apparent K_M , k_{cat} , and the second-order rate constant (k_{cat}/K_M) are summarized in Table 2 along with the previously reported values (27) for the phosphorolytic reaction measured using the same assay.

Values of k_{cat} for the arsenolytic and phosphorolytic reactions were similar at 22 °C and 37 °C. The K_M values for dT are similar at 22 °C, but at 37 °C, dT shows fourfold lower affinity with saturating arsenate than with phosphate. Dependence of affinity for dT on the nucleophile supports the report that phosphate binding causes conformational changes to form the active site in the structurally related *E. coli* thymidine phosphorylase (40). Differences in AsO_4 and PO_4 size and charge cause changes in the active site that translate into the differences in dT affinity.

Commitments to Catalysis

KIEs measured by the competitive label method give the apparent isotope effect on k_{cat}/K_M and reflect all steps from free reactants through the first irreversible step (41). These include contributions from non-chemical steps, steps that achieve equilibrium during the reaction, and are frequently manifesting as commitments to catalysis (42). Intrinsic KIEs can be approached by corrections for commitment factors.

Isotope effect studies on the N-ribosyltransferases are usually influenced by large commitments to catalysis. Arsenate is often useful to reduce commitments in these systems (19,43,44). The product of arsenolysis, ribose 1-arsenate, is unstable and rapidly hydrolyzes to ribose and arsenate (45). Hydrolysis prior to product release prevents internal reversibility, thus removing the reverse commitment. A decrease in the rate of the chemical step can shift the rate-determining step from a non-chemical one. A decrease in the affinity of enzyme for labeled substrate or product would lead to a reduction in the commitments.

KIE measurements for hTP arsenolysis were made at a variety of temperatures, and at 22 °C partial suppression of KIEs was observed (data not shown). Similar experiments were performed at 37 °C showing more significant expression of KIEs (Table 3). Traditionally, a forward commitment has been assessed with isotope trapping, but low affinity of hTP for dT in the absence of an inorganic ester and the presence of an alternate hydrolytic activity make such measurements impossible (data not shown) (27). Computational analysis (see below) revealed that the experimental $1-^{15}N$ KIE of 1.018 was within experimental error of the maximum theoretical KIE for this position (1.020). Thus, masking of the experimental KIEs by commitment factors at 37 °C must be small and the observed KIE approximates the intrinsic KIE.

KIEs for dT Arsenolysis

Intrinsic KIEs reflect the nature of the transition state at the kinetically significant (rate-determining) chemical step (41,42). Measurement of multiple KIEs for substrates provides information related to transition state structure. KIE measurements were made on multiple labeled substrates for the hTP-catalyzed arsenolytic depyrimidination of dT (Table 3).

1'-¹⁴C KIE

Primary ¹⁴C KIEs for N-glycoside hydrolysis and transfer reactions report on the extent of oxocarbenium ion character at the transition state. Values on the order of 1.00 to 1.03 are expected for reactions involving well-developed oxocarbenium ion transition states and of 1.080 to 1.13 for associative concerted bimolecular reactions with neutrally charged pentavalent transition states (17). The value observed for hTP arsenolysis of 1.025 indicates significant oxocarbenium ion character at the chemical step.

1-¹⁵N KIE

The extent of C1'-N1 bond cleavage is related to the primary ¹⁵N KIE and lies between unity for early (substrate like) transition states and the equilibrium isotope effect (EIE) for late (product like) transition states (41). The value of 1.018 indicates considerable C1'-N1 bond cleavage and is in agreement with the 1'-¹⁴C KIE which demonstrates significant oxocarbenium ion character during the reaction.

1'-³H KIE

Support for a well-developed oxocarbenium ion-character in the arsenolytic reaction is given by the α -secondary ³H KIE and is consistent with other enzyme-catalyzed N-glycoside bond cleavage reactions demonstrating this characteristic. A range of 1.15 to 1.34 for α -secondary ³H KIEs is typical in oxocarbenium ion-like transition states (22). Rehybridization at C1' from sp³ in the reactant to sp² in the transition state gives increased freedom to the out-of-plane bending mode of H1' resulting in the large normal KIE (46,47). The value of 1.177 is significantly lower than observed for hTP hydrolysis (1.325) (27). hTP hydrolysis was established to react via a D_N*A_N[‡] mechanism. A steric effect from the leaving group or attacking AsO₄ (absent in the TS for the hydrolytic reaction) may contribute to the observed decrease in the α -secondary KIE. This would support a dissociative A_ND_N mechanism for hTP arsenolysis.

2'-³H KIEs

The magnitudes of the β -secondary KIEs give geometric information on the ribose ring at the transition state. The oxocarbenium ion exhibits significant π -bonding character in the O4'-C1' bond, favoring coplanarity between the C4'-O4'-C1'-C2' atoms. Hyperconjugation between the C2'-H2' σ -bond and the vacant p-orbital of C1' can increase π -bonding character in the C1'-C2' bond and weaken the C2'-H2' σ -bond, resulting in a looser bonding environment for the H2' hydrogen and an increasing normal KIE with optimization of orbital alignment (18,48). This phenomenon stabilizes the positive charge on the anomeric carbon in the oxocarbenium ion. The low values observed for both 2'*R*-³H (1.028) and 2'*S*-³H (1.048) are unusual and indicate limited hyperconjugation at the TS. KIEs at this position for related N-glycosides with 2'-deoxyribose sugars are not widely documented, but show a trend of significant hyperconjugation to both 2' hydrogens, with KIEs ranging from 1.08 to 1.15 (23,25,26). Other related reactions have indicated the absence of stabilizing hyperconjugative forces from the 2' position at the transition state (43,49,50). Binding

³A similar model was presented in transition state analysis of the hydrolysis reaction catalyzed by hTP, where the imidazole was shown to activate the water nucleophile in the rate-determining transition state.

isotope effects or steric compression by active site residues at the transition state may diminish the apparent KIE, and these effects must also be considered.

The KIE measurements described here point to a transition state with extensive oxocarbenium ion character at the transition state. Computational matching of the experimental KIEs is required for a definitive mechanistic conclusion.

DISCUSSION

$A_N D_N$ Mechanism and Predicted KIEs

This mechanism invokes simultaneous participation of the nucleophile (arsenate) and the leaving group (thymine) in the rate-limiting transition state. A previous theoretical study on a structurally related enzyme (TP from *E. coli*) proposed a key role for an active site histidine in the activation of phosphate and stabilization of a thymine anion by hydrogen bonding (51). Mutation of the analogous residue in hTP renders the enzyme catalytically inactive (52). We therefore incorporated a histidine mimic (imidazole) along with dT and arsenate in the computational analysis of the experimental KIEs.³

The KIEs of the atoms involved in the reaction coordinate ($1'-^{14}\text{C}$, $1'-^3\text{H}$ and $1'-^{15}\text{N}$) are primary indicators of transition state structure. A potential energy surface was generated by restraining the distances along the reaction coordinate, namely the breaking C-N bond ($r_{\text{C-N}}$) and the forming C-O bond ($r_{\text{C-O}}$).⁴ The best match between model and intrinsic KIEs corresponded to geometries where $r_{\text{C-N}}$ ranged from 2.5 – 2.9 Å and $r_{\text{C-O}}$ from 3.0 – 2.5 Å (Scheme 1) and when the sum of these distances was 5.4 Å. These geometries correspond to a dissociative transition state with significant oxocarbenium ion character. Several transition structures based on these select geometries were located by varying the orientation of arsenate and thymine with respect to the 2-deoxyribose ring. The predicted KIEs for these geometries led to a final transition state model within the framework of an $A_N D_N$ mechanism (Fig. 3). It provided the best match of experimental and theoretical KIEs.

The dissociative $A_N D_N$ transition state exhibits significant oxocarbenium ion character, with a weak N-ribosidic bond ($r_{\text{C-N}} = 2.45$ Å) and almost no significant bond order to the attacking nucleophile ($r_{\text{C-O}} = 2.95$ Å) (Fig. 3). Favorable hydrogen bonds between the imidazole, the nucleophile and the leaving group determines their orientation with respect to the ribocation.⁵ The heavy atom KIE predictions ($1'-^{14}\text{C}$ and $1'-^{15}\text{N}$) are within the uncertainty of the experimental KIE measurements. The key $1'-^3\text{H}$ KIE, which is sensitive to both reaction coordinate motion and steric effects enforced by the active site, is well predicted in this model. α -Secondary KIEs are often over-predicted since most computational models do not include contributions from the neighboring enzymatic groups. Including imidazole in this model provides an important step to improve the accurate modeling of this isotope effect.⁶

The KIEs that report on the ring-pucker of the 2'-deoxyribose ring, namely the $2'-^3\text{H}(R)$ and $2'-^3\text{H}(S)$ KIEs, are reasonably well predicted. Even though the calculations correctly predict a larger KIE for the (*S*) than the (*R*) hydrogen, the $2'-^3\text{H}(S)$ KIE is over-predicted by 14%

⁴For a detailed description of the preliminary model and the predicted KIEs see Supporting Information.

⁵The hydrogen bond between the nitrogen atom of the histidine and the -OH of the arsenate activates the nucleophile. The anionic leaving group thymine is stabilized by a second hydrogen bond between the protonated nitrogen of histidine and O2 of thymine. A similar model, with hydrogen bonding to N1 instead of O2 at the transition state, over-predicts the ^{15}N KIE (1.026) supporting anionic leaving group stabilization by hydrogen bonding to O2 (Figure 3). Extending the argument, if thymine leaves as a neutral protonated species (as opposed to the anion at N1 stabilized by hydrogen bonding to O2), it is likely that the 1,2-lactim tautomer of thymine would be the initial product.

⁶An identical transition state geometry *without* the histidine interaction gave a prediction of 30% for this KIE, almost double the experimental KIE of 17%.

(1.188 versus the experimental KIE of 1.048). The most plausible explanation is that the KIEs for one of the two 2'-hydrogens is suppressed by factors that are not included in our theoretical model. Steric compression by an active-site residue is a reasonable hypothesis for this effect since: (1) hTP is selective for 2'-deoxy substrates indicating that the active site is crowded when a bulkier group is at this position (53), and (2) a similar phenomenon was observed in the prediction of KIEs for the hydrolytic reaction catalyzed by hTP where, at a geometry where *all* KIEs were consistent with experiment, the 2'-³H(*S*) KIE was over-predicted by nearly 5% (27). The observation that this effect is more pronounced in arsenolysis than in hydrolysis is also expected, as the binding of phosphate (and by analogy arsenate) causes a conformational change resulting in a domain closure around the active site (40). The low 2'-³H(*R*) KIE of 1.028 suggests that the transition state does not involve much overlap with this orbital and supports a mild 2'-endo transition structure (Fig. 3). The anticipated large 2'-³H(*S*) KIE is suppressed by interactions with the active site.

This transition state has low bond order to both the nucleophile and the leaving group (Fig. 3). We explored the effect of having only one of the two species participating at the rate limiting transition state, i.e. the possibility of a stepwise mechanism. The $D_N^{\ddagger}A_N$ (rate-limiting dissociation of thymine forming an oxocarbenium ion intermediate captured by arsenate at a subsequent step) or $D_N^*A_N^{\ddagger}$ (reversible dissociation of thymine followed by rate-limiting capture of the oxocarbenium ion intermediate by arsenate) stepwise mechanisms were considered with and without the active site histidine (Schemes 2 and 3).

Stepwise Mechanisms and Predicted KIEs

For the $D_N^{\ddagger}A_N$ mechanism, dissociation of thymine was modeled by varying r_{C-N} between 2.3 and 2.7 Å at increments of 0.1 Å. Each fixed distance geometry was optimized and frequency calculations performed. KIEs were calculated based on the single imaginary frequency corresponding to C-N bond cleavage (Table 4). Predicted KIEs for this mechanism are inconsistent with experiments. At longer C-N distances the 1'-¹⁴C KIEs are close to the experimental value of 1.025, but at these distances the 1'-³H KIE is larger due to the increased amplitude of the out-of-plane C-H bending mode. Including histidine (Scheme 2B) reduces this KIE, but the value is still 1.495, compared to the experimental value of 1.177. At short C-N distances the prediction for the 1'-³H KIE is in closer agreement (experimental value of 1.275), but the 1'-¹⁴C KIE of 1.048 is not well predicted.⁷ These observations do not support the $D_N^{\ddagger}A_N$ mechanism.⁸

A $D_N^*A_N^{\ddagger}$ stepwise mechanism warrants scrutiny since the hTP-catalyzed hydrolytic reaction is characterized by this mechanism (27). Water is not the native nucleophile, resulting in an increased barrier for oxocarbenium ion capture. The hydrolytic transition state in best agreement with experimental KIEs involved reversible formation of thymine (lactam form) followed by capture of the oxocarbenium ion intermediate by an activated water nucleophile in the rate-limiting step.

A $D_N^*A_N^{\ddagger}$ stepwise mechanism for arsenolysis predicts the KIE to be a product of the EIE for formation of the oxocarbenium ion and the intrinsic KIE for oxocarbenium ion capture by arsenate. The A_N^{\ddagger} step was modeled with and without the active site histidine mimic, by varying r_{C-O} between 2.2 and 2.7 Å at fixed increments of 0.1 Å (Scheme 3; Table 5). These

⁷Primary ¹⁴C KIEs are typically smaller than secondary ³H KIEs and can usually be predicted within ± 0.003 of the experimental value. Secondary ³H KIEs are sensitive to the environment around the hydron and a prediction within ± 0.05 of the experimental measurement is considered a good match.

⁸The orientation of thymine with respect to the 2-deoxyribose ring was found to have an effect on the predicted 1'-¹⁴C and 1'-³H KIEs. For making a reasonable comparison with the A_N^{\ddagger} model, the dihedral angle defined by C2-N2-1'C-2'C was fixed in the optimizations for the $D_N^{\ddagger}A_N$ model with the histidine mimic.

predicted KIEs show dependence of the 1'-¹⁴C KIEs on the nature of the nucleophile. At identical distances for the forming C-O bond, the 1'-¹⁴C KIEs are larger for histidine-activated arsenate than arsenate alone. When the predicted and experimental 1'-¹⁴C KIE are similar, the predicted 1'-³H KIE is significantly higher than experiment with or without the histidine mimic. The predicted KIEs for both stepwise mechanisms are inconsistent with the experimental measurements.

Proposed Mechanism

Intrinsic KIEs establish that the arsenolytic depyrimidination of dT by hTP proceeds via a concerted $A_N D_N$ mechanism with a dissociative transition state and significant oxocarbenium ion character. While common for *N*-ribose hydrolysis and transfer reactions, it is the first $A_N D_N$ mechanism for a reaction with a 2'-deoxyribose. A $D_N^* A_N^\ddagger$ mechanism is observed for the hydrolytic activity of hTP (27). A minimal kinetic mechanism and a qualitative free energy diagram can be proposed (Fig. 4).

A transition state with hydrogen bonding interactions between an active site histidine and both the departing thymine and attacking arsenate give the best match to the experimental KIEs. Stabilization of the leaving group and activation of the nucleophile result from these interactions. Similar interactions were predicted to facilitate catalysis in a molecular dynamics study of the structurally related *E. coli* thymidine phosphorylase (51). The conserved active site histidine serves a similar role in the human enzyme.

Protonation at N1 in the leaving group does not accurately predict the experimentally observed KIEs, suggesting N1 is likely not being protonated at the transition state. Hydrogen bonding to O2 by the active site histidine withdraws electron density and reproduces the KIEs. This raises the possibility that thymine leaves as a stabilized N1 anion. A related enzymatic reaction, uracil DNA glycosylase, catalyzes formation of a stabilized N1 anion of uracil in an analogous step (23). Protonation of O2 by the active site histidine to form the 1,2-lactim tautomer of thymine, cannot be ruled out. Leaving group protonation at the transition state occurs at N7 of adenine in the MutY-catalyzed hydrolytic depurination of DNA (25). In hTP hydrolysis, product thymine is rapidly protonated at N1 and this species equilibrates with the transition state, therefore occurring in a reversible step with oxocarbenium ion formation. Protonation at N1 explains the on-enzyme equilibrium between N1-protonated thymine and free reactant, which occurs before a rate limiting capture of the oxocarbenium ion by water. Similar chemistry is proposed to occur immediately after leaving group departure in arsenolysis. It is therefore proposed that after departure of the leaving group, hTP catalyzes the formation of N1-protonated thymine through general acid base chemistry (Figure 4). In the case of the N1 anion this would be direct protonation at N1, and in the case of the 1,2-lactim tautomer of thymine, an enzyme catalyzed tautomerization would occur.

Previous Arsenolytic Study

A previous study of the arsenolysis reaction catalyzed by hTP reported a near-symmetric $A_N D_N$ nucleophilic transition state with bond orders near 0.5 to both the nucleophile and the leaving group (32). This conclusion was based on a large [1'-¹⁴C]dT KIE with smaller KIEs from the α - and β -³H effects. These isotope effects and conclusions on transition state structure differ substantially from the present experiments. The differences in the transition states is apparent from a More O'Ferrall-Jencks plot comparing the present $D_N^* A_N^\ddagger$ transition state with that reported earlier (32) (Fig. 5). The transition state reported here for arsenolysis and that reported earlier for dT hydrolysis by hTP, using the same native hTP preparation, are related, as both proceed via ribocation formation (Fig. 5).

The previous experiments were performed with hTP constructed and expressed with purification tags. More recent results linking protein dynamic architecture to transition state structure establish that mutations remote from the catalytic site are capable of altering transition state structure, providing one possible explanation for the departure from earlier work (55). In hTP, the effects may be more direct. Structures of hTP show the active sites near the dimer subunit interface. The N-terminal helices form this interface, thus the N-termini are near the catalytic sites (52). The sensitivity of transition state structure to structural and environmental changes argues for using the most physiological conditions available when transition state analysis is intended to guide inhibitor design.

Effects Contributing to Chemical Mechanism

Transition state analysis of the arsenolysis reaction provides an opportunity to compare hydrolysis (weak nucleophile) with a nucleophile (arsenate) more closely related to phosphate. The hydrolytic reaction is characterized by a stepwise $D_N^*A_N^\ddagger$ mechanism with rate-limiting capture of the oxocarbenium ion intermediate by a water nucleophile hydrogen bonded to histidine (Fig. 2). With water, the A_N step is the first irreversible step, and an equilibrium is established between the high energy oxocarbenium ion intermediate and free reactant. Conversely, arsenolysis proceeds by a concerted bimolecular mechanism, though hydrogen bonding interactions to the reacting nucleophile provides similarity for both catalytic activities. This shift in chemical mechanism is apparent in a More O'Ferrall-Jencks plot (Fig. 5).

The slightly larger volume of arsenate and altered pKa relative to phosphate raises the question of the effect of the nucleophile on transition state structure. At the transition state there is only weak bonding interactions between the attacking nucleophile and the ribocation, thus we propose these differences to be minimal. As the rates of arsenolysis and phosphorolysis are similar, despite differences in their chemical reactivity, we propose that the rate of nucleophile addition is governed by migration of the highly reactive deoxyribocation toward enzyme-bound nucleophile, a common mechanism in the N-ribosyltransferases.

This fundamental shift in the chemical mechanism between hydrolysis and arsenolysis is caused by the relatively poor nucleophilicity of water when bound into a catalytic site designed to bind phosphate. Altered nucleophilicity in solution chemistry also promotes the shift from concerted to stepwise mechanisms.

CONCLUSIONS

hTP catalyzes the arsenolytic depyrimidination of dT, chemistry similar to the physiological phosphorolytic activity. The catalytic turnover numbers for arsenolysis and phosphorolysis reactions are similar. However the affinity of dT for hTP•arsenate is fourfold lower than for hTP•phosphate. hTP catalysis involves a transition state exhibiting significant ribooxocarbenium ion character. At the transition state, there is more bond order in the N-ribosidic bond ($r_{C-N} = 2.45 \text{ \AA}$) than to the attacking nucleophile ($r_{C-O} = 2.95 \text{ \AA}$). An active site histidine (His 116) is proposed to participate at the transition state to bridge the nucleophile and leaving group in a hydrogen bonding network. This catalytic site interaction activates the attacking arsenate and stabilizes the departing thymine. During the $A_N D_N$ step, thymine leaves as an anionic species lacking a proton on N1 and general acid base chemistry is proposed to rapidly convert it to N1 protonated thymine.

Supplementary Material

Refer to Web version on PubMed Central for supplementary material.

References

1. Friedkin M, Roberts D. The enzymatic synthesis of nucleosides. I. Thymidine phosphorylase in mammalian tissue. *J Biol Chem.* 1954; 207:245–256. [PubMed: 13152099]
2. Krenitsky TA, Koszalka GW, Tuttle JV. Purine nucleoside synthesis, an efficient method employing nucleoside phosphorylases. *Biochemistry.* 1981; 20:3615–3621. [PubMed: 6789872]
3. Krenitsky TA. Pentosyl transfer mechanisms of the mammalian nucleoside phosphorylases. *J Biol Chem.* 1968; 243:2871–2875. [PubMed: 5653178]
4. Zimmerman M. Deoxyribosyl Transfer: II. Nucleoside:pyrimidine deoxyribosyltransferase activity of three partially purified thymidine phosphorylases. *J Biol Chem.* 1964; 239:2622–2627. [PubMed: 14235545]
5. Miyazono K, Okabe T, Urabe A, Takaku F, Heldin CH. Purification and properties of an endothelial cell growth factor from human platelets. *J Biol Chem.* 1987; 262:4098–4103. [PubMed: 3549724]
6. Ishikawa F, Miyazono K, Hellman U, Drexler H, Wernstedt C, Hagiwara K, Usuki K, Takaku F, Risau W, Heldin CH. Identification of angiogenic activity and the cloning and expression of platelet-derived endothelial cell growth factor. *Nature.* 1989; 338:557–562. [PubMed: 2467210]
7. Brown NS, Bicknell R. Thymidine phosphorylase, 2-deoxy-D-ribose and angiogenesis. *Biochem J.* 1998; 334(Pt 1):1–8. [PubMed: 9693094]
8. Hotchkiss KA, Ashton AW, Schwartz EL. Thymidine phosphorylase and 2-deoxyribose stimulate human endothelial cell migration by specific activation of the integrins alpha 5 beta 1 and alpha V beta 3. *J Biol Chem.* 2003; 278:19272–19279. [PubMed: 12639965]
9. de Bruin M, Smid K, Laan AC, Noordhuis P, Fukushima M, Hoekman K, Pinedo HM, Peters GJ. Rapid disappearance of deoxyribose-1-phosphate in platelet derived endothelial cell growth factor/thymidine phosphorylase overexpressing cells. *Biochem Biophys Res Commun.* 2003; 301:675–679. [PubMed: 12565833]
10. Takebayashi Y, Natsugoe S, Baba M, Akiba S, Fukumoto T, Miyadera K, Yamada Y, Takao S, Akiyama S, Aikou T. Thymidine phosphorylase in human esophageal squamous cell carcinoma. *Cancer.* 1999; 85:282–289. [PubMed: 10023693]
11. Foher F, Spadari S. Thymidine phosphorylase: a two-face Janus in anticancer chemotherapy. *Curr Cancer Drug Targets.* 2001; 1:141–153. [PubMed: 12188887]
12. Foth H, Hellkamp J, Kunellis EM, Kahl GF. Pulmonary elimination and metabolism of 5-fluoro-2'-deoxyuridine in isolated perfused rat lung and lung slices. *Drug Metab Dispos.* 1990; 18:1011–1017. [PubMed: 1981506]
13. Cole C, Foster AJ, Freeman S, Jaffar M, Murray PE, Strafford IJ. The role of thymidine phosphorylase/PD-ECGF in cancer chemotherapy: a chemical perspective. *Anticancer Drug Des.* 1999; 14:383–392. [PubMed: 10766293]
14. Fukushima M, Suzuki N, Emura T, Yano S, Kazuno H, Tada Y, Yamada Y, Asao T. Structure and activity of specific inhibitors of thymidine phosphorylase to potentiate the function of antitumor 2'-deoxyribonucleosides. *Biochem Pharmacol.* 2000; 59:1227–1236. [PubMed: 10736423]
15. de Bruin M, van Capel T, Van der Born K, Kruyt FA, Fukushima M, Hoekman K, Pinedo HM, Peters GJ. Role of platelet-derived endothelial cell growth factor/thymidine phosphorylase in fluoropyrimidine sensitivity. *Br J Cancer.* 2003; 88:957–964. [PubMed: 12644837]
16. Schramm VL. Enzymatic transition state poise and transition state analogues. *Acc Chem Res.* 2003; 36:588–596. [PubMed: 12924955]
17. Berti PJ, Tanaka KS. Transition state analysis using multiple kinetic isotope effects: mechanisms of enzymatic and non-enzymatic glycoside hydrolysis and transfer. *Adv Phys Org Chem.* 2002; 37:239–314.
18. Parkin DW, Mentch F, Banks GA, Horenstein BA, Schramm VL. Transition-state analysis of a Vmax mutant of AMP nucleosidase by the application of heavy-atom kinetic isotope effects. *Biochemistry.* 1991; 30:4586–4594. [PubMed: 2021651]
19. Kline PC, Schramm VL. Purine nucleoside phosphorylase. Catalytic mechanism and transition-state analysis of the arsenolysis reaction. *Biochemistry.* 1993; 32:13212–13219. [PubMed: 8241176]

20. Berti PJ, Blanke SR, Schramm VL. Transition state structure for the hydrolysis of NAD catalyzed by diphtheria toxin. *J Am Chem Soc.* 1997; 119:12079–12088. [PubMed: 19079637]
21. Bates C, Kendrick Z, McDonald N, Kline PC. Transition state analysis of adenosine nucleosidase from yellow lupin (*Lupinus luteus*). *Phytochemistry.* 2006; 67:5–12. [PubMed: 16300810]
22. Berti PJ, McCann JA. Toward a detailed understanding of base excision repair enzymes: transition state and mechanistic analyses of N-glycoside hydrolysis and N-glycoside transfer. *Chem Rev.* 2006; 106:506–555. [PubMed: 16464017]
23. Werner RM, Stivers JT. Kinetic Isotope Effect Studies of the Reaction Catalyzed by Uracil DNA Glycosylase: Evidence for an Oxocarbenium Ion–Uracil Anion Intermediate. *Biochemistry.* 2000; 39:14054–14064. [PubMed: 11087352]
24. McCann JAB, Berti PJ. Transition State Analysis of Acid-Catalyzed dAMP Hydrolysis. *J Am Chem Soc.* 2007; 129:7055–7064. [PubMed: 17497857]
25. McCann JAB, Berti PJ. Transition-State Analysis of the DNA Repair Enzyme MutY. *J Am Chem Soc.* 2008; 130:5789–5797. [PubMed: 18393424]
26. Chen XY, Berti PJ, Schramm VL. Transition-State Analysis for Depurination of DNA by Ricin A-Chain. *J Am Chem Soc.* 2000; 122:6527–6534.
27. Schwartz PA, Veticatt MJ, Schramm VL. Transition State Analysis of Thymidine Hydrolysis by Human Thymidine Phosphorylase. *J Am Chem Soc.* 2010; 132:13425–13433. [PubMed: 20804144]
28. Booker S, Stubbe J. Cloning, sequencing, and expression of the adenosylcobalamin-dependent ribonucleotide reductase from *Lactobacillus leichmannii*. *Proc Natl Acad Sci U S A.* 1993; 90:8352–8356. [PubMed: 8397403]
29. Merkler DJ, Kline PC, Weiss P, Schramm VL. Transition-state analysis of AMP deaminase. *Biochemistry.* 1993; 32:12993–13001. [PubMed: 8241153]
30. Shi W, Tanaka KS, Crother TR, Taylor MW, Almo SC, Schramm VL. Structural analysis of adenine phosphoribosyltransferase from *Saccharomyces cerevisiae*. *Biochemistry.* 2001; 40:10800–10809. [PubMed: 11535055]
31. Parkin DW, Leung HB, Schramm VL. Synthesis of nucleotides with specific radiolabels in ribose. Primary ¹⁴C and secondary ³H kinetic isotope effects on acid-catalyzed glycosidic bond hydrolysis of AMP, dAMP, and inosine. *J Biol Chem.* 1984; 259:9411–9417. [PubMed: 6746654]
32. Bircck MR, Schramm VL. Nucleophilic Participation in the Transition State for Human Thymidine Phosphorylase. *J Am Chem Soc.* 2004; 126:2447–2453. [PubMed: 14982453]
33. Parkin, DW. Enzyme mechanism from isotope effects. Cook, PF., editor. CRC Press, Inc; Boca Raton, FL: 1991. p. 269-290.
34. Lewis BE, Schramm VL. Conformational equilibrium isotope effects in glucose by (¹³C) NMR spectroscopy and computational studies. *J Am Chem Soc.* 2001; 123:1327–1336. [PubMed: 11456704]
35. Lewis BE, Schramm VL. Binding equilibrium isotope effects for glucose at the catalytic domain of human brain hexokinase. *J Am Chem Soc.* 2003; 125:4785–4798. [PubMed: 12696897]
36. Becke AD. Density-functional thermochemistry. III. The role of exact exchange. *J Chem Phys.* 1993; 98:5648–5652.
37. Hirschi JS, Takeya T, Hang C, Singleton DA. Transition-state geometry measurements from (¹³C) isotope effects. The experimental transition state for the epoxidation of alkenes with oxaziridines. *J Am Chem Soc.* 2009; 131:2397–2403. [PubMed: 19146405]
38. Anisimov V, Paneth PJ. ISOEFF98. A program for studies of isotope effects using Hessian modifications. *J Math Chem.* 1999; 26:75–86.
39. Bell, RP. *The Tunnel Effect in Chemistry.* Chapman & Hall; London: 1980.
40. Pugmire MJ, Cook WJ, Jasanoff A, Walter MR, Ealick SE. Structural and theoretical studies suggest domain movement produces an active conformation of thymidine phosphorylase. *J Mol Biol.* 1998; 281:285–299. [PubMed: 9698549]
41. Cook, PF.; Cleland, WW. *Enzyme Kinetics and Mechanism.* Garland Science; New York: 2007.
42. Northrop DB. The expression of isotope effects on enzyme-catalyzed reactions. *Annu Rev Biochem.* 1981; 50:103–131. [PubMed: 7023356]

43. Lewandowicz A, Schramm VL. Transition state analysis for human and *Plasmodium falciparum* purine nucleoside phosphorylases. *Biochemistry*. 2004; 43:1458–1468. [PubMed: 14769022]
44. Singh V, Schramm VL. Transition-State Structure of Human 5'-Methylthioadenosine Phosphorylase. *J Am Chem Soc*. 2006; 128:14691–14696. [PubMed: 17090056]
45. Parks, RE., Jr; Agarwal, RP. *The Enzymes*. Boyer, PD., editor. Academic Press; New York: 1972. p. 483-514.
46. Glad SS, Jensen F. Transition State Looseness and a-Secondary Kinetic Isotope Effects. *J Am Chem Soc*. 1997; 119:227–232.
47. Matsson, O.; Westaway, KC. Secondary Deuterium Kinetic Isotope Effects and Transition State Structure. In: Bethell, D., editor. *Adv Phys Org Chem*. Academic Press; San Diego: 1998. p. 143-248.
48. Sunko DE, Szele I, Hehre WJ. Hyperconjugation and the angular dependence of. beta-deuterium isotope effects. *J Am Chem Soc*. 1977; 99:5000–5005.
49. Singh V, Lee JE, Nunez S, Howell PL, Schramm VL. Transition state structure of 5'-methylthioadenosine/S-adenosylhomocysteine nucleosidase from *Escherichia coli* and its similarity to transition state analogues. *Biochemistry*. 2005; 44:11647–11659. [PubMed: 16128565]
50. Chen XY, Berti PJ, Schramm VL. Ricin A-Chain: Kinetic Isotope Effects and Transition State Structure with Stem-Loop RNA. *J Am Chem Soc*. 2000; 122:1609–1617.
51. Mendieta J, Martin-Santamaria S, Priego EM, Balzarini J, Camarasa MJ, Perez-Perez MJ, Gago F. Role of Histidine-85 in the Catalytic Mechanism of Thymidine Phosphorylase As Assessed by Targeted Molecular Dynamics Simulations and Quantum Mechanical Calculations†. *Biochemistry*. 2003; 43:405–414. [PubMed: 14717594]
52. Mitsiki E, Papageorgiou AC, Iyer S, Thiyagarajan N, Prior SH, Sleep D, Finnis C, Acharya KR. Structures of native human thymidine phosphorylase and in complex with 5-iodouracil. *Biochem Biophys Res Commun*. 2009; 386:666–670. [PubMed: 19555658]
53. Pugmire MJ, Ealick SE. Structural analyses reveal two distinct families of nucleoside phosphorylases. *Biochem J*. 2002; 361:1–25. [PubMed: 11743878]
54. Schramm VL. Enzymatic transition state theory and transition state analogue design. *J Biol Chem*. 2007; 282:28297–28300. [PubMed: 17690091]
55. Luo M, Li L, Schramm VL. Remote mutations alter transition-state structure of human purine nucleoside phosphorylase. *Biochemistry*. 2008; 47:2565–2576. [PubMed: 18281957]

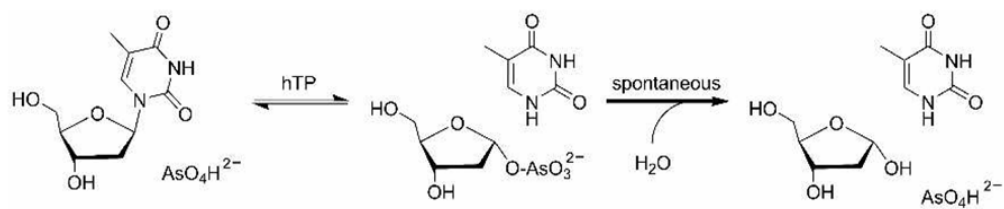


Figure 1.
hTP-catalyzed arsenolytic depyrimidination of dT.

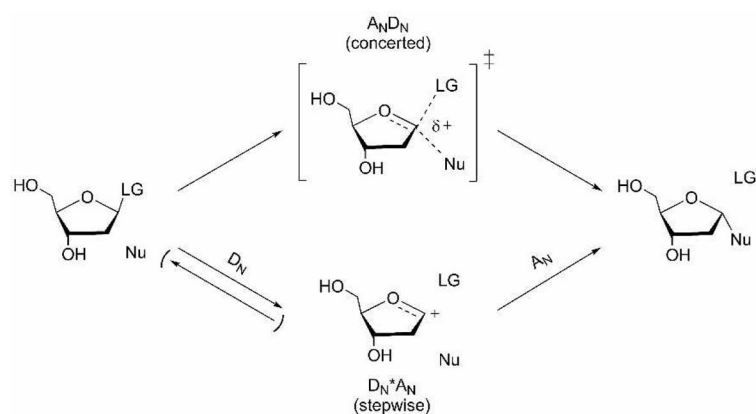


Figure 2. Generic mechanism for glycosidic bond cleavage of ribofuranosides. In the upper pathway, attack from the nucleophile (Nu) displaces the leaving group (LG) in a concerted bimolecular process ($A_N D_N$). In the lower pathway, departure of LG occurs in an independent step (D_N) from attack of the 2-deoxyribose oxocarbenium ion by Nu (A_N). In a $D_N^\ddagger A_N$ mechanism, the D_N step is rate-limiting. In a $D_N^* A_N^\ddagger$ mechanism, the A_N step is rate-limiting, and the glycosidic bond cleaves and reforms many times before nucleophilic capture.

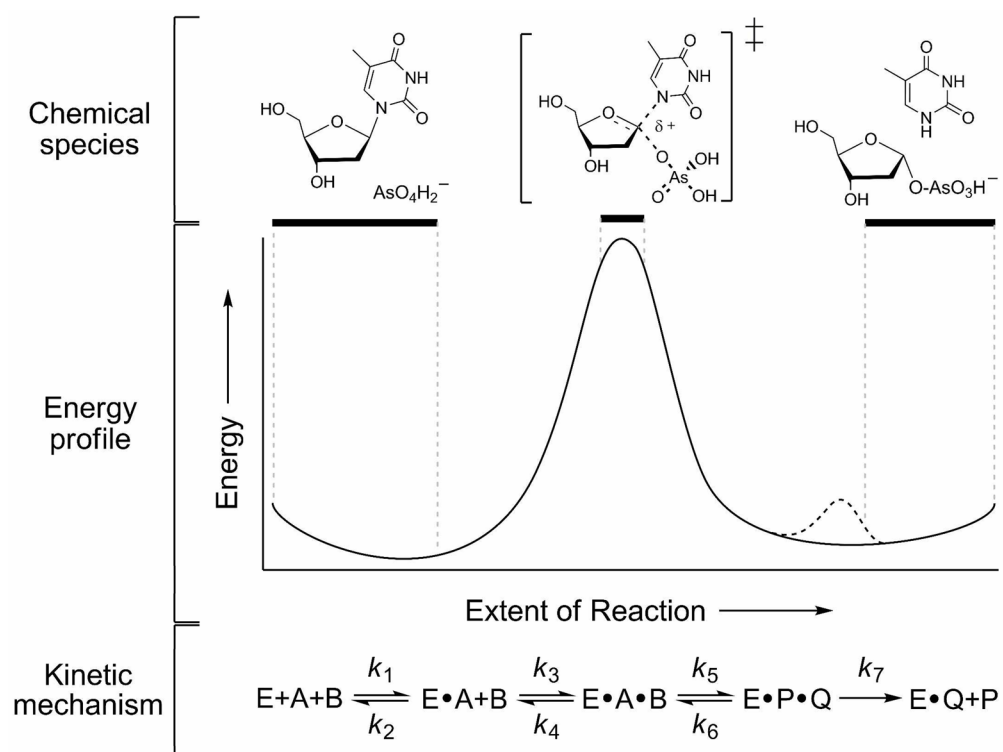


Figure 4.

Chemical and kinetic mechanism of the hTP-catalyzed arsenolytic depyrimidination of dT. In the proposed mechanism the nucleophilic arsenate displaces the departing thymine in a concerted process. At the transition state the ribose has significant oxocarbenium character. (upper panel) The chemical species present at specific stages of catalysis. (middle panel) Free energy profile for enzyme catalyzed chemistry represented qualitatively. The proposed protonation step (see text) is represented by the dashed line (- -). (lower panel) The minimal kinetic mechanism through release of the first product: E, enzyme free in solution; A or B, substrate free in solution; E•A, binary substrate complex; E•A•B, ternary substrate complex; E•P•Q, ternary product complex; E•Q, binary product complex; P or Q, product free in solution; k_n , rate constant on step n . Catalysis is likely more complex, containing conformational changes after substrate binding and general acid/base chemistry after nucleophilic displacement.

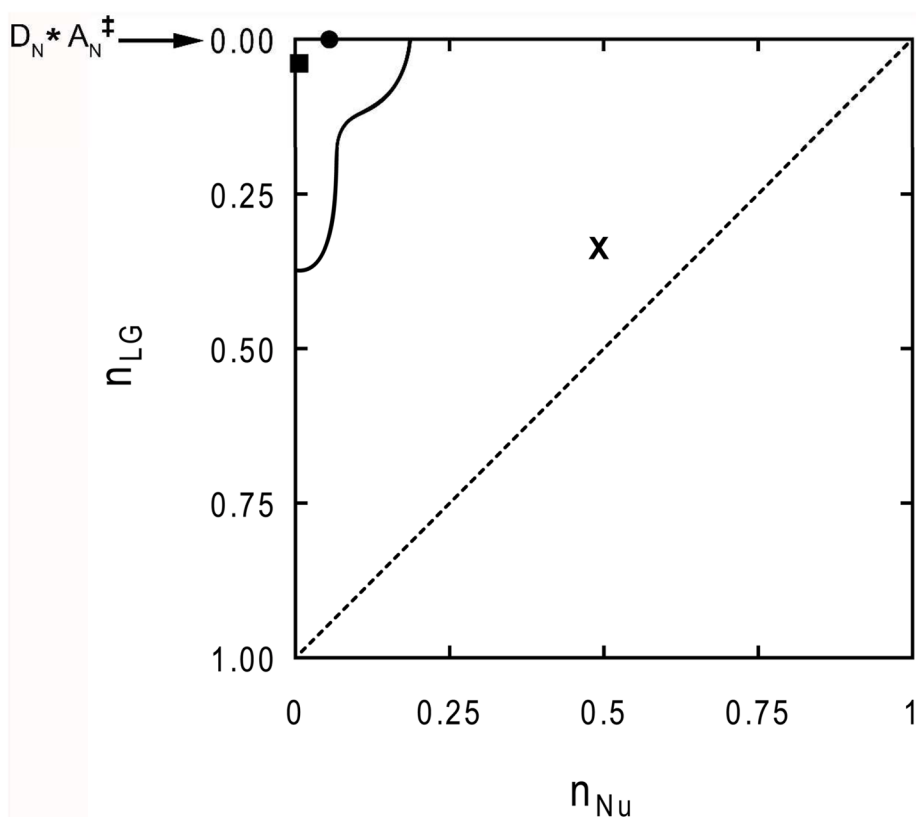
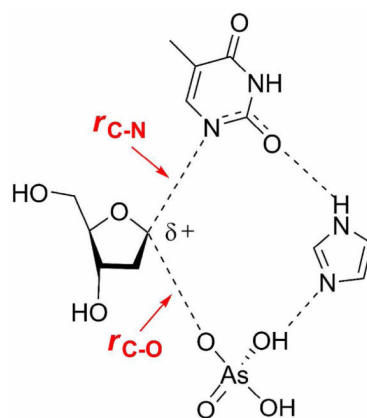
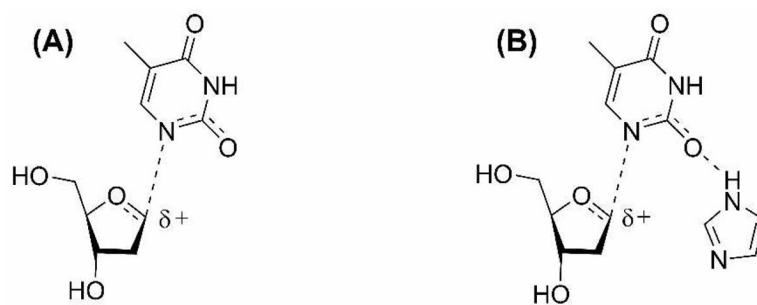


Figure 5. Reaction space for *N*-ribose hydrolysis and transfer reactions. The axes are the Pauling bond order from the nucleophile (X-axis) or the leaving group (Y-axis) to the anomeric carbon, C1'. (X) Near-symmetric synchronous transition state for hTP arsenolysis as previously determined (32). (■) Transition state for hTP arsenolysis proposed from the current study. In this mechanism, the leaving group is nearly dissociated as the nucleophile begins to capture the anomeric carbon. (●) Recently identified transition state for the hTP-catalyzed hydrolytic depyrimidination of dT (27). In this mechanism, the nucleophile captures an oxocarbenium ion intermediate in the step after leaving group departure. Stepwise $D_N^*A_N^\ddagger$ reactions lie on the axis at $n_{LG} = 0$. The dashed line (- -) represents the interface between associative and dissociative transition states of concerted processes, with synchronous mechanisms falling on the line. The solid line (—) encompasses the area that related enzyme-catalyzed reactions occupy (for which TS analysis has been performed). Graph adapted from elsewhere (22,54).



Scheme 1.



Scheme 2.

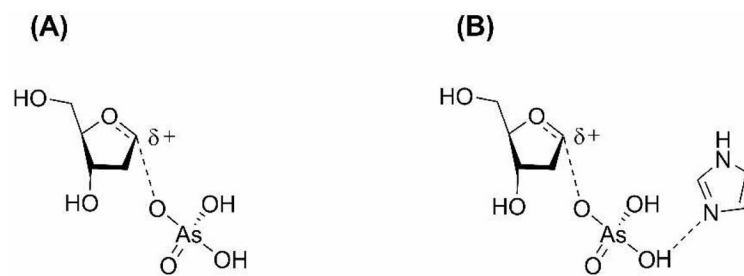
**Scheme 3.**

Table 1

Radiolabeled starting material used to synthesize isotopically enriched thymidines and remote labels used in KIE experiments.

radiolabeled thymidine	starting material	remote label
[1'- ¹⁴ C]dT	[1- ¹⁴ C]ribose	[5'- ³ H]dT
[1- ¹⁵ N, 5'- ¹⁴ C]dT	[6- ¹⁴ C]glucose ^a	[5'- ³ H]dT
[1'- ³ H]dT	[1- ³ H]ribose	[5'- ¹⁴ C]dT
[2' <i>R</i> - ³ H]dT	[2 <i>R</i> - ³ H]-2-deoxyribose	[5'- ¹⁴ C]dT
[2' <i>S</i> - ³ H]dT	[2 <i>S</i> - ³ H]-2-deoxyribose	[5'- ¹⁴ C]dT
[5'- ³ H]dT	[6- ³ H]glucose	[5'- ¹⁴ C]dT
[5'- ¹⁴ C]dT	Commercially available	n.a. ^b

^a 1-¹⁵N labeled thymine was also used in the synthesis.

^b The KIE of [5'-¹⁴C]dT is assumed to be unity (see text).

Table 2

Steady state kinetic parameters for the arsenolytic and phosphorolytic depyrimidination of dT by hTP.

condition ^a	k_{cat} (s ⁻¹)	K_{M} dT ^{b, c} (μM)	K_{M} nucleophile ^{b, c} (μM)	$k_{\text{cat}}/K_{\text{M}}$ ^d (M ⁻¹ s ⁻¹)
Phosphorolysis, 22 °C ^e	2 ± 0.1	31 ± 6	5 ± 0.6	(6.7 ± 1.3) × 10 ⁴
Arsenolysis, 22 °C	3 ± 0.1	60 ± 4	5 ± 0.9	(5 ± 0.4) × 10 ⁴
Phosphorolysis, 37 °C ^e	7 ± 0.2	30 ± 4	11 ± 2	(2.3 ± 0.3) × 10 ⁵
Arsenolysis, 37 °C	8 ± 0.4	112 ± 15	29 ± 7	(7.3 ± 1) × 10 ⁴

^ahTP was incubated at 22 °C and 37 °C and steady state kinetic parameters determined as described.

^bNucleophile is PO₄ in phosphorolysis and AsO₄ in arsenolysis.

^cApparent K_{M} was determined for varying concentrations of substrate at a saturating concentration of the other substrate.

^d $k_{\text{cat}}/K_{\text{M}}$ value listed is for dT at saturating concentrations of the nucleophilic substrate.

^eData from Ref. 32.

Table 3

Experimental competitive KIEs for the arsenolytic depyrimidination of dT by hTP.

labeled dT	type of KIE	apparent KIE ^{a, b}
[1'- ¹⁴ C]dT	primary ¹⁴ C	1.025 ± 0.003 (2) ^c
[1- ¹⁵ N, 5'- ¹⁴ C]dT	primary ¹⁵ N	1.018 ± 0.002 (2) ^c
[1'- ³ H]dT	α-secondary ³ H	1.177 ± 0.002 (2)
[2' <i>R</i> - ³ H]dT	β- <i>(R)</i> -secondary ³ H	1.028 ± 0.001 (2)
[2' <i>S</i> - ³ H]dT	β- <i>(S)</i> -secondary ³ H	1.048 ± 0.003 (2)
[5'- ³ H]dT	δ-secondary ³ H	1.019 ± 0.002 (2)

^aThe number in parentheses is the number of independent KIE experiments.

^bThe experimentally measured KIE for the position of interest (corrected for remote label where noted) is equal to the apparent KIE (see text).

^cKIEs were corrected for the remote ³H label according to the expression: $KIE_{app} = KIE_{obs} \times KIE_{remote}$, where KIE_{app} is the apparent KIE for the position of interest, KIE_{obs} is the experimentally measured KIE, and KIE_{remote} is the observed KIE for the remote label.

Table 4

Predicted KIEs along the reaction coordinate for a $D_N^{\ddagger}A_N$ mechanism.^a

KIE position	r_{C-N} (Å)						
	2.7	2.6	2.5	2.4	2.3	2.2	2.1
1- ¹⁴ C	1.031	1.032	1.036	1.043	1.048		
1- ¹⁴ C + His ^b	1.029	1.030	1.035	1.041	1.048		
1- ¹⁵ N	1.025	1.025	1.025	1.025	1.025		
1- ¹⁵ N + His ^b	1.023	1.023	1.024	1.024	1.024		
1- ³ H	1.686	1.551	1.452	1.366	1.307		
1- ³ H + His ^b	1.495	1.412	1.369	1.321	1.275		

^aKIEs were computed using ISOEFF98 at 310.15 K. No correction for tunneling was incorporated.

^bKIEs of the model incorporating an active site histidine mimic.

Table 5

Predicted KIEs^a along the reaction coordinate for a $D_N^*A_N^\ddagger$ mechanism^b 3

KIE position	r_{C-O} (Å)						
	2.2	2.3	2.4	2.5	2.6	2.7	
1- ¹⁴ C	1.040	1.031	1.026	1.019	1.013	1.012	
1- ¹⁴ C + His ^b	1.059	1.054	1.048	1.044	1.040	1.035	
1- ³ H	1.246	1.284	1.319	1.358	1.378	1.406	
1- ³ H + His ^b	1.232	1.277	1.321	1.359	1.391	1.418	

^aThe KIEs shown in this table are a product of the EIE for the DN step and the intrinsic KIE for the AN step.

^bKIEs were computed using ISOEFF98 at 310.15 K. No correction for tunneling was incorporated.

^cKIEs of the model incorporating an active site histidine mimic.